IAC-16.A6.2.8x35593

DEBRISAT FRAGMENT CHARACTERIZATION SYSTEM AND PROCESSING STATUS

M. Rivero, B. Shiotani, M. Carrasquilla[1]

N. Fitz-Coy[1], J.-C. Liou[2], M. Sorge[3], T. Huynh[4], J. Opiela[5], P. Krisko[5], and H. Cowardin[6]

[1]The University of Florida, USA, [2]National Aeronautics and Space Administration, USA, [3]The Aerospace Corporation, USA, [4]United States Air Force/Space and Missile Systems Center, USA, [5]Jacobs JETS, USA, **[6]**University of Texas at El Paso - JETS

The DebriSat project is a continuing effort sponsored by NASA and DoD to update existing break-up models using data obtained from hypervelocity impact tests performed to simulate on-orbit collisions. After the impact tests, a team at the University of Florida has been working to characterize the fragments in terms of their mass, size, shape, color and material content. The focus of the post-impact effort has been the collection of 2 mm and larger fragments resulting from the hypervelocity impact test. To date, in excess of 125K fragments have been recovered which is approximately 40K more than the 85K fragments predicted by the existing models. While the fragment collection activities continue, there has been a transition to the characterization of the recovered fragments. Since the start of the characterization effort, the focus has been on the use of automation to (i) expedite the fragment characterization process and (ii) minimize the effects of human subjectivity on the results; e.g., automated data entry processes were developed and implemented to minimize errors during transcription of the measurement data. At all steps of the process, however, there is human oversight to ensure the integrity of the data. Additionally, repeatability and reproducibility tests have been developed and implemented to ensure that the instrumentations used in the characterization process are accurate and properly calibrated.

I. BACKGROUND

The Satellite Orbital debris Characterization Impact-Test (SOCIT) hypervelocity impact test was performed in 1992 using a 1960s Navy Transit satellite as part of a test series. Data from this test and from radar observation of the space environment lead to the formulation of standard break-up models that NASA and the U.S. Department of Defense (DoD) use to predict orbital debris populations for in-orbit debris generating events such as collisions. The standard break-up models have performed well in predicting debris populations from older satellites and rocket bodies which have similar material compositions to the Navy Transit satellite. However, a number of recent collision events have raised concerns that the standard break-up models may be outdated and in need of fresh data samples. The most prominent of these collision events was the 2009 collision between the Iridium-33 satellite and the defunct Cosmos-2251 satellite. Post-impact radar observations of the resulting debris fields revealed that the standard break-up models accurately predicted the debris population from Cosmos2251 but did not accurately predict the debris population from Iridium33. The error in the model's prediction has been attributed to the use of materials and components in the Iridium satellite not accounted for in the break-up model[1]. To address these inaccuracies of the standard break-up models, NASA and the DoD launched an effort to update the models with modern satellite materials and components. This effort is the DebriSat project, centered on a 56-kg satellite (Fig. 1) developed to be representative of materials and components found in most modern low Earth orbit (LEO) satellites. DebriSat was subject to a hypervelocity impact test in the spring of 2014[1].
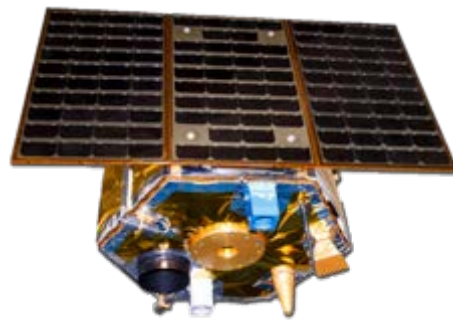

Fig. 1 DebriSat

In the 24 months since the impact test the DebriSat team has been focused on the effort to collect and characterize the debris fragments. Past papers presented at the International Astronautical Congress (IAC) have described the design of DebriSat[2], the fabrication and hypervelocity test of DebriSat[1], and the initial fragment characterization effort[3]. This installment of the DebriSat papers provides updates on the characterization process

focused on increasing automation to expedite the fragment characterization process and to minimize human-induced errors.

II.POST-IMPACT TASK OVERVIEW

There are three main tasks for the post-impact processing of the DebriSat fragments: Detection, Extraction and Characterization. Each task has associated sub-tasks and activities in order to accomplish the tasks as shown in Fig. 2

As described in Ref. [1], in an effort to minimize damage to the fragments generated by the hypervelocity impact, the walls of the test chamber were covered with polyurethane foam panels to form a "soft-catch arena."

For fragment detection each foam panel is prepared for X-ray image acquisition by collecting loose and embedded fragments on the surfaces of the panels. Once preparation is completed, the panels are X-rayed and the X-ray images post-processed to detect embedded fragments.

The extraction task involves carefully recovering embedded fragments from the panels utilizing results from the X-ray images. Prior to extracting fragments, each panel is verified to ensure that the preparation data is properly input to the DebriSat Categorization System (DCS). The DCS is a database solution that was designed and developed to manage the large amounts of data generated by DebriSat[4]. Once panels are verified, they are ready for fragment extraction. Fragments with at least one dimension greater than 2mm are carefully extracted and recorded into the DCS and given unique identification numbers and barcodes. Due to the large amount of data associated with each individual debris fragment multiplied by the massive number of debris, the use of unique identification numbers and barcodes is critical in the characterization process. Utilizing unique identifiers, each fragment's data can be accessed and retrieved from the DCS any time during post-impact processing and analysis.

The characterization task for each fragment includes assessment, measurement, and calculation. There are four types of assessments: size, material, shape, and color. For measurement, there are two types: mass and size. The measurement data are used to calculate the characteristic length, volume, average cross-sectional area, and area-to-mass ratio. The characteristic length is defined as the average of the fragment's largest three orthogonal dimensions. Once characterization data is entered in the DCS, each fragment is verified to ensure that the recorded data is accurate.

To ensure the integrity of the data generated from this project, the research technicians are rigorously and comprehensively trained prior to participation in any of the post-impact tasks. Furthermore, repeatability and reproducibility tests were designed and implemented, where the repeatability tests are to ensure that the

instrumentations used in the characterization process are precise and the reproducibility tests are to ensure that the entire process is technician independent. Both the repeatability and reproducibility tests are conducted at set intervals and are described in subsequent sections.
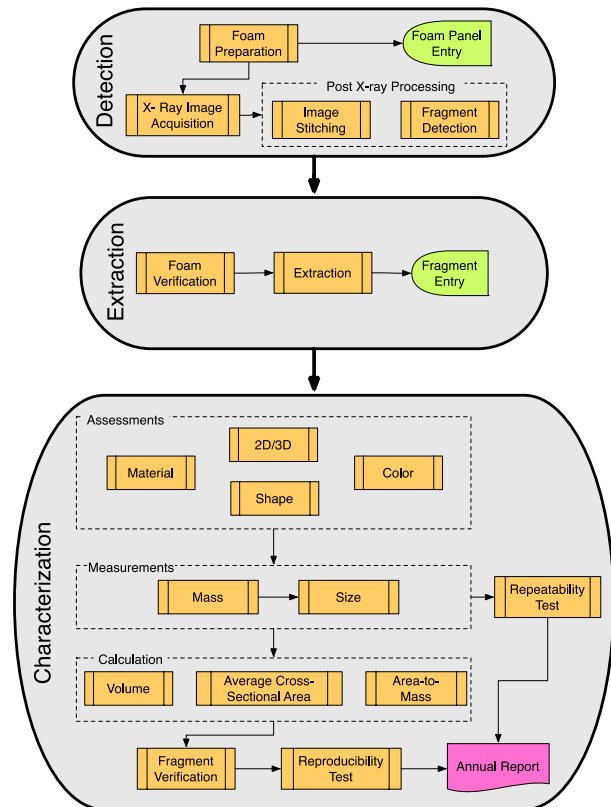

Fig. 2 Post-impact task workflow

III. CHARACTERIZATION PROCESS

During the fragment characterization process, parameters such as the material, shape, color, mass, and size are assessed and/or measured. Utilizing these parameters, characteristics such as the characteristic length, volume, average cross-sectional area, and area-to-mass ratio are computed. Additional parameters can be determined post-project by utilizing archived data including images of the fragments. The characterization process is categorized into two main activities: assessment and measurement. Once fragments are characterized, a verification process is used to certify that the data in the database are valid. In this section, each activity is discussed in detail.

III.I Assessment

The characterization process begins by performing assessments on the fragment. The size, material, shape, and color of the fragment are qualitatively assessed and entered in the DCS. Each of the assessment fields in the DCS is displayed in a drop-down list to avoid any

variations due to manual inputs. Each assessment is discussed in this section.

Size assessment

One of the requirements for the fragment size measurement is to keep the characteristic length errors less than 10%, where the characteristic length is defined as the average of the fragment's largest three orthogonal dimensions. Since a significant portion of the fragments are needles/slivers (see Fig. 3) or flat plates (see Fig. 4) two size categories were defined: 2D objects and 3D objects. Examples of a needle/sliver fragment and a flat plate fragment are shown in Fig. 5 and Fig. 6, respectively. Furthermore, the shape definitions are addressed in the Shape assessment section. Utilizing the requirement, analytical expressions for the characteristic length error were derived for needle/sliver fragments and thin plate-like fragments (i.e., 2D fragments) and are shown in equations [1] and [2], respectively. Utilizing these analytical expressions, the errors were computed and analyzed. The 2D error analysis results are shown in Table 1 and the 3D error analysis results are shown in Fig. 7 and Table 2.
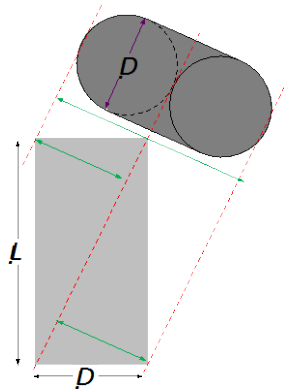

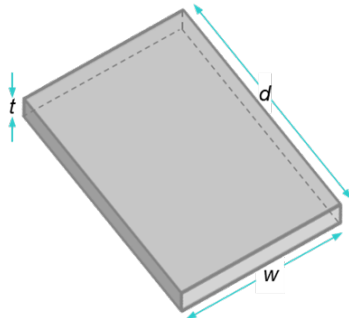**Fig. 3 Dimensions for a needle/sliver fragment**

Fig. 4 Dimensions for a flat plate fragment

Fig. 5 Picture of a needle/sliver fragment

Fig. 6 Picture of a flat plate fragment

$$0 \geq 100(100 - 2n)\chi^4 - 4n^2\chi^3 \qquad [1]$$

where $\chi = \dfrac{D}{L}$ and $n = error\ percent$.

$$n = 1 - \frac{\left(\sqrt{1 + \delta^2} + \dfrac{2\delta}{\sqrt{1 + \delta^2}} \right)}{\left(\sqrt{1 + \delta^2 + \tau^2} + 2\delta \dfrac{\sqrt{1 + \tau^2}}{\sqrt{1 + \delta^2 + \tau^2}} + \dfrac{2\tau}{\sqrt{1 + \tau^2}} \right)} \qquad [2]$$

where $\delta = \dfrac{d}{w}$ .and $\tau = \dfrac{t}{w}$

Table 1 Results from 2D error analysis

Error (%)	D/L
10	0.143
7	0.080
5	0.058
3	0.033
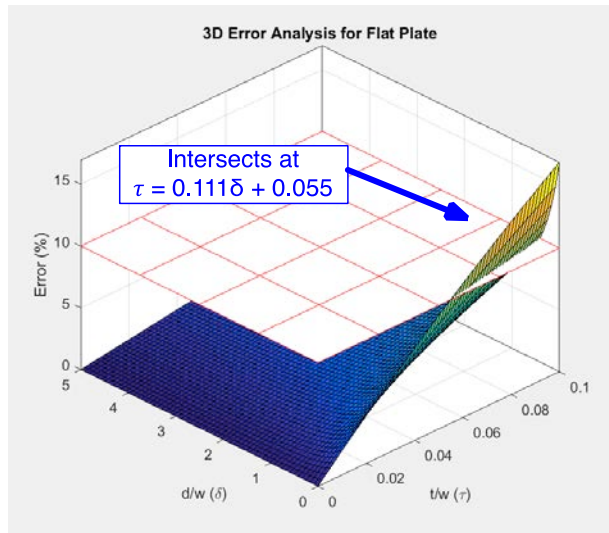
Fig. 7 Error analysis for 3D fragments (e.g., flat plate fragments)

Table 2 Results from 3D error analysis

δ	τ
0	0.055
0.1	0.066
0.2	0.077
0.3	0.088
0.4	0.099

For needle-like fragments, if the length is seven or more times its width (i.e., $L > 7D$), the fragment qualifies as 2D. For flat plate type fragments, if the thickness is less than 25% of the length (i.e., $t < 0.25d$), then the fragment qualifies as a 2D fragment. Based on these results, the fragments are characterized and organized as either 2D or 3D and entered into the DCS.

Material assessment
The list of materials used in the fabrication of DebriSat, their designation in the database, and their associated densities are provided in Table 3. The technician assesses the material content of a fragment by comparing to samples and then inputs the result into the DCS; a drop down list on the user interface is utilized to standardize the selection options. These samples include spare materials from the construction of DebriSat as well as images of specific materials.

Shape assessment
Fragments are categorized into six different shapes as shown in Table 4. The shape categories are based on the input from the Satellite Orbital debris Characterization Impact Test (SOCIT)[5], shapes observed from the DebriSat fragments, and input from subject matter experts. The fragment's assessed shape is also entered into the DCS using a drop down list on the user interface.

Table 3 Material list and their densities

Base Material	DCS Designator	Density (g/cm³)
Aluminum	-AL-	2.700
Carbon Fiber Reinforced Polymer (CFRP)	-CFRP-	1.550
Copper	-CU-	8.938
Epoxy	-EPOXY-	1.050
GLASS	-GLASS-	2.510
Kapton Tape	-KAP-	1.420
Kevlar	-KEV-	1.440
Multi-layered Insulation (MLI)	-MLI-	0.772
Printed Circuit Board (PCB)	-PCB-	1.860
Plastic	-Plastic-	1.250
Solar cells UTJ	-SCEL-	5.320
Silicone	-SIL-	1.080
Stainless Steel	-SS-	7.900
Titanium	-TI-	4.400

Table 4 Shape categories for DebriSat

Name	Definition
Straight rod/needle/cylinder	¼ of the longest solid-body dimension is greater or equal to the second longest solid-body dimensions (L/W ≥ 4)
Bent rod/needle/cylinder	Same as straight rod/needle/cylinder and 25% of the longest dimension is bent more than 45°.
Flat plate	Longest solid body dimension is less than 4 times the second longest body dimension and the third longest dimension is less than ¼ of the second longest dimension.
Bent plate	Same as flat plate but the 25% of the longest dimension is bent more than 45°.
Nugget/parallelepiped /spheroid	Longest solid body dimension is less than 4 times the second longest dimension and the third longest dimension is more than ¼ of the second longest dimension.
Flexible	Fragments that easily change shape.

Color assessment
During development of DebriSat, each bay of the satellite was assigned a specific color and aluminum

components in that bay were anodized to that color to aid in the characterization process. The bay color assignment for DebriSat is shown in Fig. 8. A list of colors was generated utilizing the bay color assignments, colors from components (e.g., cable sheaths) in DebriSat, and colors observed from DebriSat fragments. The color options available to choose from in the DCS are:

- Black
- Clear (Glass)
- Green
- Gold
- Light Blue
- Magenta
- Orange
- Purple
- Red
- Royal Blue
- Silver
- White
- Yellow
- Burnt/Charred

Utilizing the list of colors, the technicians assess the color of the fragments and a drop down list on the DCS user interface is utilized to standardize the selection options.
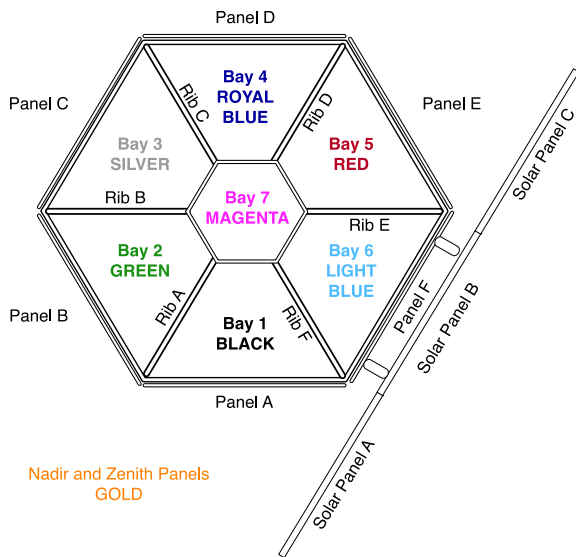

Fig. 8 DebriSat bay color assignment

Figure 9 shows an example where the technician has completed the assessment of a fragment and has entered the appropriate data into the DCS user interface.

III.II Measurement

Once assessments are completed, the fragment's physical characteristics (i.e., mass and size) are measured. Details of the measurement processes are discussed in the following sub sections.
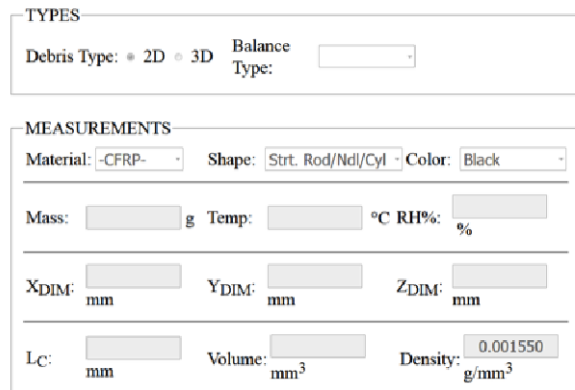

Fig. 9 Screen capture of the DCS user interface with assessments completed

Mass measurement

Three mass balances have been selected to perform the mass measurements. Table 5 shows the specifications for the selected mass balances.

Table 5 Summary of mass balances used for mass measurement

Model	Capacity (g)	Readability (g)	Std. Dev. (g)
BM-22	5	0.000001	0.000004
PGL 203	200	0.001	0.002
CY-510	510	0.001	0.001

A significant portion (>75%) of the fragments that have been collected are very small, thus requiring the use of a microbalance. The BM-22 microbalance from A&D Engineering meets the measurement requirements but is extremely sensitive and the slightest disturbances can cause variations in measurements. Potential disturbances include vibrations and physical impacts, environmental variations (temperature, humidity, and air pressure), static electricity, and body heat from the technicians. To reduce the effects of vibrations and physical impacts, the microbalance was placed on a granite table. To reduce the effects from changes in the environment, a draft shield was used. To account for the static discharges, an anti-static mat was also placed on the granite table. The setup is shown in Fig. 10.

The most challenging factor in the precision mass measurements was thermal variations due to heat emitted from humans in the presence of the instrumentation. In order to acclimate the microbalance to the environment of the room with a technician present, the microbalance mass measurement procedure includes a stabilization time (around 10 to 15 minutes) prior to operating the microbalance. The current setup on the granite table includes three balances, one microbalance and two milligram balances (PGL203 and CY-510). For the larger

debris fragments, mass measurements can be accomplished with a regular laboratory scale.
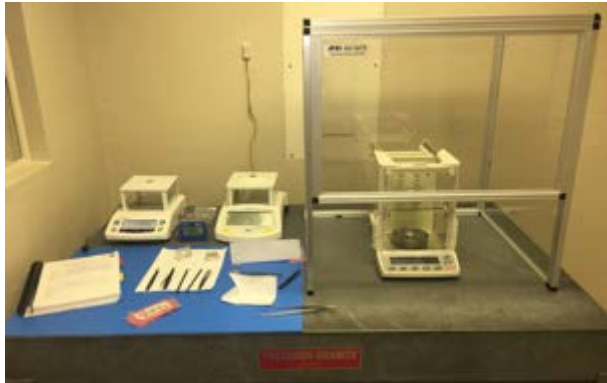

Fig. 10 Microbalance setup on granite table

Another data requirement is to record the temperature and humidity at the time of each mass measurement. In order to satisfy this requirement, a temperature and humidity sensor was placed near the balances. In order to minimize human intervention on the data acquisition process, the integrated mass measurement system (instruments, temperature and humidity sensor, DCS, and barcode scanner) is connected via a serial interface to a graphical user interface (GUI). Fig. 11 shows a diagram of the integrated system. Each balance has a serial interface which the GUI utilizes to read the mass measurements. Additionally, the temperature and humidity sensors are integrated with an Arduino-based processor that has a serial interface to communicate with the GUI. The measurements are then automatically uploaded to the DCS database. A screen capture of the mass measurement GUI is shown in Fig. 12.
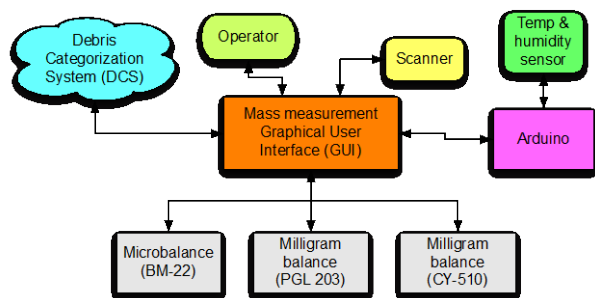

Fig. 11 Integrated mass measurement system block diagram

The mass measurement procedure has been rigorously developed and implemented. Due to the sensitivity of the micro mass balance, the technicians are trained to take extra precautions during the use of the microbalance. For example, the amount of time the door for the microbalance is kept open is minimized and the technicians are required to use long tweezers to place the weighing boat inside the chamber to avoid putting their hands inside. Additionally, the GUI is setup such that if the balance does not re-zero within tolerance after each fragment's mass is captured, the measurement is deemed invalid and is not uploaded to the DCS database. In such cases, the technician is required to re-weigh the fragment.
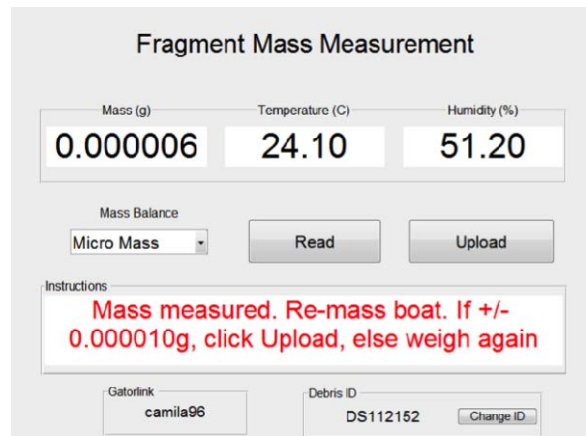

Fig. 12 Screen capture of the mass measurement GUI

Size measurement

After mass measurements have been completed, the fragments are ready to be imaged in the 2D or 3D imaging systems to determine their size. To overcome challenges of measuring fragile and –unique/non-standard geometrical shaped fragments, two imaging systems were developed; 2D and 3D imaging systems. Both imaging systems have automated characteristic length measurements driven by the need to quickly and accurately measure tens of thousands of debris fragments. Furthermore, both imaging systems acquire images, create representative point clouds, determine the characteristic length, and upload the data into the DCS database. These imaging systems reduce handling of debris fragments to a minimum as well as any human error during characteristic length measurements.

During size assessments, the fragments are organized into 2D or 3D container bins. The container bins represent the corresponding imaging system used to perform the size measurement. The 2D measurement process involves computing the two largest in-plane dimensions through the use of a single 2D image, acquired by the 2D imaging system. The 2D imaging system consists of a single Canon PowerShot S110 camera, an imaging platform with LED lights controlled by an Arduino, a barcode scanner, a shroud, and a computer with the 2D imaging GUI. The shroud serves two purposes; blocks external light and minimizes air perturbations that may cause the fragment to move during the imaging process. The 2D imaging system setup and the block diagram are shown in Fig. 13 and Fig. 14, respectively. First, the technician scans the fragment's

barcode into the 2D imaging GUI and carefully places the fragment and a calibration ring on the imaging boat under the camera. The calibration ring is used to compute the pixel-to-millimeter ratio which is then utilized in the fragment size measurement. The 2D imaging GUI communicates with the camera and acquires two images of the fragment (one with all lights and the other with only the base light). The LED lights on the platform are controlled through the Arduino. From the acquired images, the software determines the outline of the fragment and creates a 2D point cloud. The two longest orthogonal dimensions are determined from this point cloud. From the two longest dimensions, the characteristic length is computed[6]. In addition to the characteristic length, the volume, average cross-sectional area, and the area-to-mass ratio are calculated. Data produced from the 2D imaging system is automatically uploaded to the DCS database. Provisions are made on the 2D imaging GUI such that if database fields on the DCS are not populated, the results from the 2D imaging system cannot be uploaded. A screen capture of the 2D imaging GUI is shown in Fig. 15.
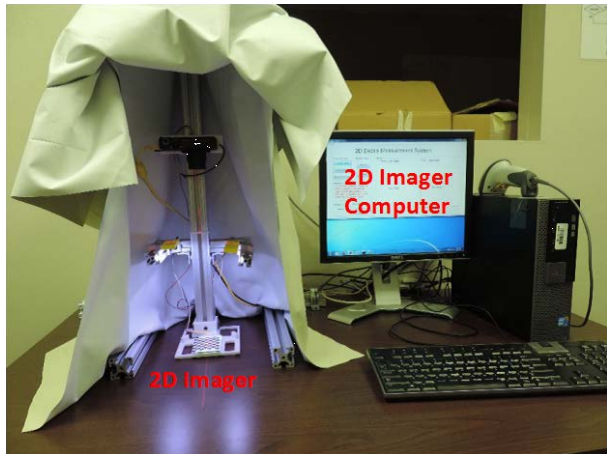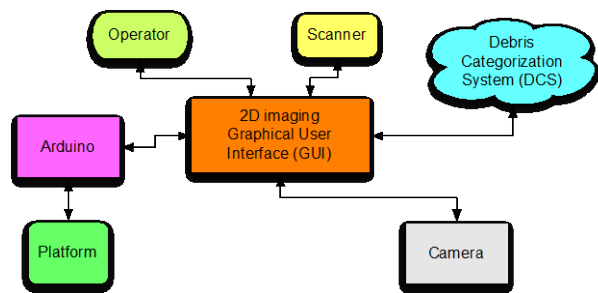

Fig. 13 Two-dimensional imaging system setup

Fig. 14 Two-dimensional imaging system block diagram
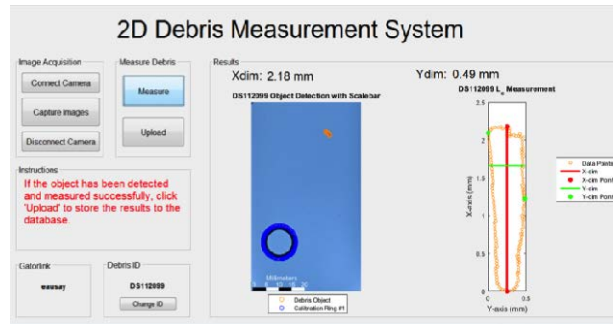

Fig. 15 Two-dimensional imaging GUI

Fragments that have been categorized as 3D objects from the size assessments are processed using the 3D imaging system. The 3D imaging system consists of six point and shoot cameras, a green-screen turntable controlled by an Arduino, three light boxes, and a computer with the 3D imaging GUI. The six cameras are distributed (18 degrees apart) along a vertical arch providing varied elevations relative to the fragment. The turntable rotates the object through multiple azimuths for a full 360-degree view of the object[7]. The setup of the 3D imaging system is shown in Fig. 16.
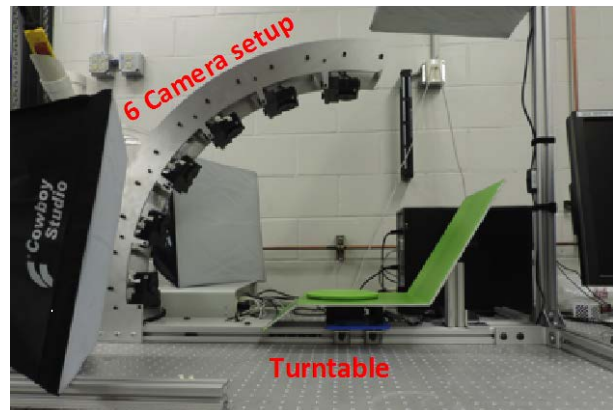
Fig. 16 Three-dimensional imaging system setup

The 3D processing involves constructing a 3D representation from multiple 2D images utilizing a space carving technique[8]. The 2D images are acquired from various azimuth and elevation angles around the object to provide the data needed for the 3D reconstruction. A checkerboard pattern is used to identify the camera parameters, such as orientation, position, focal length, and others. From the camera parameters, the pixel-to-millimeter ratio is computed and used in the size measurement.

The 3D imaging GUI communicates with the cameras and the Arduino to acquire multiple 2D images. All the images are used in the space carving algorithm to produce the 3D point cloud representation of the fragment. The three largest orthogonal dimensions are determined from the point cloud using a convex hull

algorithm. Utilizing the three largest orthogonal dimensions, the characteristic length of the object is calculated. Furthermore, the volume, the bulk density, the average cross-sectional area, and the area-to-mass ratio are computed.

Images and calculated data results are automatically uploaded to the DCS database. A block diagram of the 3D imaging system is shown in Fig. 17. Currently, the 3D imaging GUI and the software are being finalized.
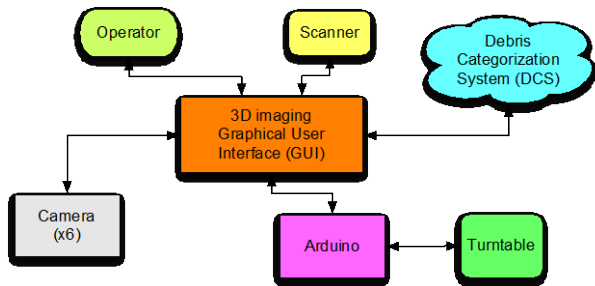

Fig. 17 Three-dimensional imaging system block diagram

Once the mass and size measurements are taken and the characteristic length of the fragment is computed, additional parameters are derived. These parameters include the volume, bulk density, average cross-sectional area, and area-to-mass ratio. The average cross sectional area is the average of the projected surface areas over all orientations[9] and is used to calculate the area-to-mass ratio. All calculated and derived parameters along with images captured by the measurement systems are automatically uploaded and archived on the DCS database. Because of the database's storage, these data can easily be further post-processed and utilized in updating the standard break-up models.

Fragment verification

After the fragments are characterized, each fragment goes through a verification process where the technicians are required to confirm the data that is stored in the DCS database. This verification process includes checking all measurements as well as all images and point cloud files that are stored on the database. An example of the database fields that the technicians see to perform the verification is shown in Fig. 18. As an additional safeguard on the data, the technician who performs the verification cannot be a technician who performed the characterization of that fragment (assessments and/or measurements). This ensures the independence of the verification of the archived data and the images. Once the technician verifies each database field of the fragment, the technician selects the verify button on the DCS user interface. Fragments that have been verified are locked and no further data modifications/edits are allowed. Incorporating the verification process increases the

integrity of the fragment data as well as avoids accidental modifications in the future.

Fig. 18 A screen capture of the DCS database to be verified by technicians.

Measurement system validation

To ensure the validity of the measurements, the integrated mass measurement system and the 2D imaging system have been put through validation tests. The 3D imaging system hardware is developed but the software is being finalized and once completed will be subject to validation tests.

For the integrated mass measurement system, the mass measurements from the balances as well as the temperature and humidity sensors had to be validated. For the mass measurements, known calibration masses were used for each balance. Ten measurements were taken for each balance and the averages and the standard deviations were determined. The averages and the standard deviations were then compared to the specifications given by the test mass and balance manufacturers (listed as "Std. Dev." in Table 5). The specifications of the test weights are shown in Table 6. Test weight #1 was utilized for the BM-22, test weight #2 was used for PGL203 and test weight #3 was used for the CY-510. Additionally, the results from the validation tests are shown in Table 7.

Table 6 Calibration mass specifications

Test weight #	Mass (g)	Tolerance (g)
1	1	± 0.0045
2	200	± 0.16
3	500	± 0.3

Comparing the averages from Table 7 to the calibration mass specifications from Table 6, all the masses are within the stated specifications. The standard deviation difference shown in Table 7 is computed by subtracting the specified values from the measured

values. Looking at the standard deviation differences, the PGL-203 balance was the only balance that was within specification. However, the standard deviation differences for the BM-22 and the CY-510 are small enough that the differences are within the tolerances allowed by the project.

Table 7 Measurements with calibration masses

Balance	Average (g)	Std. dev. (g)	Std. dev. Difference (g)
BM-22	1.0034306	0.000005	+ 0.000001
PGL 203	199.9989	0.0011	- 0.0009
CY-510	500.012	0.004	+ 0.003

The validation of the temperature and humidity sensors involves comparing the measurements from the Arduino-based sensor to those obtained from a Supco DVTH temperature and humidity sensor. The sensors were monitored over a period of a week and the percent difference for both the temperature and the humidity readings were computed and averaged. The results are shown in Table 8.

Table 8 Temperature and humidity readings

Reading	Temperature (°C)		Humidity (%)	
	Arduino	DVTH	Arduino	DVTH
1	23.30	23.40	50.80	49.90
2	24.90	24.60	47.70	46.20
3	24.60	24.30	41.30	39.30
4	25.10	24.50	50.90	50.00
5	25.00	24.70	50.30	48.70
6	22.20	22.50	51.70	51.00
7	22.60	22.80	53.70	53.20
Average % difference	1.18 %		2.47%	

The average percent difference for the temperature and humidity readings were 1.25% and 3.18%, respectively. While neither the Arduino-based nor the DVTH sensor is calibrated, the relatively small percentage differences between their measurements provides a level of confidence in their outputs. Therefore, the team has concluded that the Arduino sensor readings are acceptable.

To validate the 2D imaging system, two sets of tests were conducted: the first set of tests was to quantify the measurement errors through accuracy testing and the second set of tests was to quantify the size limitations of the system. The accuracy testing was performed by comparing the dimensions of three calibration rings whose outer diameter (OD) and inner diameter (ID) measurements were provided by the supplier (obtained using a calibrated micrometer). Table 9 shows the dimensions of the calibration rings provided by the supplier.

Table 9 Calibration ring measurements

Ring #	OD (mm)	ID (mm)
1	12.7003	9.5341
2	12.7064	9.5298
3	12.7076	9.5382

Since the 2D imaging system computes the two longest dimensions of the object, the average outer diameter of the calibration rings was computed and compared to the known dimension of each ring (Table 9). Table 10 shows the results from this comparison.

Table 10 Ring measurement comparison

Test Ring #	Cal Ring #	X_{DIM} (mm)	Y_{DIM} (mm)	% Diff.	OD (mm)
1	ID of 3	12.79	12.76	0.23	12.78
3	ID of 1	12.77	12.75	0.16	12.76
2	ID of 3	12.80	12.72	0.63	12.76
2	OD of 3	12.86	12.78	0.62	12.82

The 2D imaging system requires a calibration object to determine the pixel-to-millimeter conversion. The second column in Table 10 lists the calibration objects (rings) used in the accuracy tests; e.g., the first row of Table 10 shows the measured dimensions of ring #1 based on the pixel-to-millimeter conversion of the ID of ring #3. While performing the accuracy test, it was observed that calibration ring #2 exhibited non-circular characteristics (the percent difference for the calibration ring #2 is higher than the other two calibration rings). Ring #2 was returned to the manufacturer and it was indeed verified to be non-circular. Calibration ring #2 is not used with the 2D imaging system. Based on these tests, the errors in the measurements of the 2D imaging system are less than 1% which is within the 10% tolerance stated in the project objectives.

Next, the 2D imaging system was tested to quantify the size limitations. Five representative fragments were used to measure the longest and the second longest dimensions (i.e., X_{DIM} and Y_{DIM}). Each sample was measured ten times to analyze the standard deviations. Furthermore, for each measurement, the sample fragment was moved within the imaging boat to remove any bias from the location of the fragment. The standard deviations of X_{DIM} and Y_{DIM} for each fragment are shown in Table 11.

Table 11 Results from size limitation test

Test Fragment	Average (mm)		Std. dev. (mm)	
	X_{DIM}	Y_{DIM}	X_{DIM}	Y_{DIM}
#1	3.89	0.85	0.03	0.03
#2	4.30	0.66	0.01	0.02
#3	5.16	2.74	0.02	0.07

#4	2.82	0.23	0.05	0.04
#5	9.62	4.49	0.19	0.83

As observed from Table 11, the 2D imaging system is capable of measuring very small fragments. Moreover the results show that the standard deviations of the fragments over ten measurements with different positions are very small for fragments #1 to #4. Unlike the other fragments, fragment #5 turned out to be a shape-changing fragment (e.g., MLI), therefore, the standard deviations were higher. To account for shape-changing fragments, the technicians use extra care when measuring these fragments and denote in the database that the fragment is flexible.

Once completed, similar tests will be performed on the 3D imaging system to quantify the accuracy and precision of the image capture/reconstruction aspects of the system.

To establish confidence in the capabilities of the algorithm that computes the characteristic length from the 3D point cloud representation of the object, NASA provided point clouds of thirteen non-DebriSat fragments for analysis. These point clouds were put through the characteristic length calculation algorithm[6,7] and the results from the algorithm were at least accurate as previous human measured characteristic lengths in all cases and more accurate in some cases. While the first revision 3D imaging system showed promising results, there were certain camera views that could not be captured with the four-camera setup. Thus, the current 3D imaging system utilizes the six-camera setup to capture all aspect angles of the object.

While validation tests show that the measurement systems satisfy the objectives, the systems must be regularly monitored to ensure the integrity of the measurements. For this, repeatability and reproducibility tests were designed and implemented.

IV. REPEATABILITY AND REPRODUCIBILITY

Prior to developing the test plans for repeatability and reproducibility, the characterization process had to be validated. For the process validation test, four technicians were randomly chosen to perform a complete characterization of five fragments (i.e. assessments, mass measurement, and size measurement). Technicians were instructed to follow the same procedures followed when conducting the characterization process. These data were analyzed and the standard deviations of each measurement were computed. To quantify the results, a Range method from Gage Repeatability and Reproducibility studies was utilized. The Range method is a quick approximation of the variability and provides an overall picture of the measurement system[10].

To calculate the gage repeatability and reproducibility (GRR) using the Range method, the range for each part is averaged, denoted as $\bar{R}$, and divided by

d_2, a tabulated value dependent on the number of tests and the product of the number of technicians and the number of parts[11]. The GRR, also known as measurement system variability, for the Range method is

$$GRR_{RANGE} = \frac{\bar{R}}{d_2} \qquad [3]$$

Using Eqn. [3], the percentage of the GRR is computed as

$$\%GRR_{RANGE} = \left(\frac{GRR}{\sigma_{process}}\right)*100 \qquad [4]$$

where $\sigma_{process}$ is the process standard deviation. The GRR percentage (%GRR) is categorized as follows: percentages below 10% indicate the system is acceptable; percentages between 10% and 30% indicate the system may be acceptable contingent upon the criteria of the project; and percentages above 30% indicate the system is unacceptable.

The characterization process validation test determined the %GRR for the integrated mass measurement system was roughly 43%. Further investigation identified the extreme sensitivity of the micro-mass balance as the root cause for the large variability between technicians. Steps to rectify this included setting aside one room solely for mass measurements, placing a draft shield over the balance, and modifying the procedures for using the micro-mass balance and with re-training personnel. Since the modifications, another process validation test was conducted and the %GRR's for the mass measurement and the 2D imager were 4.15% and 4.60%, respectively. Both results were well within the acceptable range and the characterization process is acceptable.

In order to maintain high levels of confidence in the fragment characterization data, a set of repeatability and reproducibility tests were developed and implemented. In the scope of this project, repeatability refers to the variability in the measurements of a particular fragment; in essence, repeatability testing measures the precision of the instrumentation. Reproducibility refers to the measurement variability of a particular fragment measured by different technicians; this measures the precision of the process and technicians[10-16]. The repeatability and reproducibility testing for DebriSat is derived from Gage Repeatability and Reproducibility studies. Several methods exist for the studies to analyze the measurement variability. The Range method is a quick approximation of variability and provides an overall picture of the measurement system. However, it does not decompose the variability into repeatability and reproducibility[14]. The Average and Range method is an approach which will provide a statistical estimate of both repeatability and reproducibility for a measurement system[14]. For the DebriSat repeatability and reproducibility test, both the Range method and the

Average and Range methods have been utilized to examine the measurement variability.

IV.I Range Method

In order to monitor the variability in the measurement systems, the mass balances and the 2D imaging system are tested once a month. The tests require one technician to test five different fragment samples, five tests per fragment. Since the tests are verification of the acceptability of the measurement equipment, sample fragments that are representative of the collected DebriSat fragments were used instead of the actual fragments to minimize the likelihood of damage to actual collected fragments. Using the Range method (Eqns. [3] and [4]), the variations in the measurement systems were examined.

Mass balance

The mass balance tests have only been conducted for the microbalance since, to date, only 2D carbon fiber reinforced polymer (CFRP) fragments have been characterized. Two tests have been conducted and for each test, the randomly selected technician was instructed to follow the same procedures used for performing mass measurements. The results from the tests are shown in Table 12 and for both tests, the %GRR have been 0.001% which shows that the microbalance is well within the acceptable range.

Table 12 Mass range repeatability test results

	Test 1	Test 2
Std. dev.	1.322	0.754
GRR	1.797e-5	5.084e-6
%GRR	0.001	0.001

2D imaging system

Similar to the testing of the microbalance the technicians were instructed to follow the same procedure for the 2D imaging system. Two tests have been conducted for the 2D imaging system and the results are shown in Table 13. Both results show that the 2D imaging system has %GRR less than 2%, which shows that the system is well within the acceptable range.

Table 13 Size (2D) range repeatability test results

	Test 1	Test 2
Std. dev.	4.455	4.230
GRR	0.074	0.048
%GRR	1.660	1.138

3D imaging system

As previously mentioned, the 3D imaging system is currently being finalized and once the system is in operation, tests will be conducted to examine the measurement system variation.

IV.II Average and Range Method

While tests using the Range method showed acceptable results, the Range method does not decompose the variability into repeatability and reproducibility but rather the overall system. In order to further investigate the variations, the team has decided to incorporate the Average and Range method for the future repeatability and reproducibility tests. The repeatability and reproducibility tests using the Average and Range method will be conducted for every 1000 characterized fragments.

In the Average and Range method, the measurement system repeatability is referred to as the equipment variation (EV) and the measurement system reproducibility is referred to as the appraiser variation (AV). Typically the Average and Range method suggests utilizing ten parts, three technicians, and more than two trials each. To avoid damaging the fragments, however, the DebriSat team has opted to perform the tests with five characterized fragments, three technicians and one trial per fragment. The technicians are randomly selected and perform the characterization process (i.e., assessment, mass, and size measurements) for each fragment. The results are then compared to the initially characterized data from the DCS database and analyzed for each measurement system.

From the Average and Range method, the EV and the AV are computed. Using the EV and the AV, the overall variability, or gage repeatability and reproducibility (GRR) is also determined. To analyze the GRR, the GRR percentage (%GRR) is computed. The %GRR as with the previous analysis is categorized as follows: percentages below 10% indicate the system is acceptable; percentages between 10% and 30% indicate the system may be acceptable contingent upon the criteria of the project; and percentages above 30% indicate the system is unacceptable.

As mentioned, the Average and Range method is to be implemented once more than 1000 DebriSat fragments have been characterized. The test procedure has been developed and the test is forthcoming.

V. CURRENT STATUS AND FUTURE

Since the hypervelocity impact test, approximately 125K fragments have been collected, which greatly surpassed the initial estimate of 85K debris fragments as predicted by the current satellite break-up model.

Table 14 shows the current progress (as of July 2016) since the start of the post-impact processing. Note that the number of fragments that have been collected is an estimate since not all the fragments have been recorded on the DCS database.

The majority of the work during the second year has been focused on fragment extraction and characterization. Specifically, the focus has been to work on a particular row of panels from the test chamber.

Additionally, the characterization effort to date has been using fragments that qualify as 2D and carbon fiber reinforced polymer (CFRP). The other fragments are organized into containers and are waiting to be characterized.

Table 14 Current status of post-impact process

	Year 1	Year 2
Panels prepared	304 / 564*	369 / 564*
Panels X-rayed	148	298
Panels extracted	None	62
Fragments collected	90,000	125,000
Fragments recorded in DCS	73,571	117,712
Fragments extracted	None	9344
Fragments characterized	None	882

Recent efforts, specifically the second year, are summarized in Fig. 19 and Fig. 20 which shows the panel summary and the fragment summary, respectively.
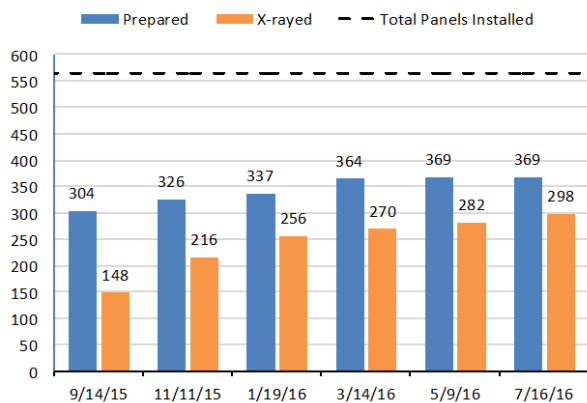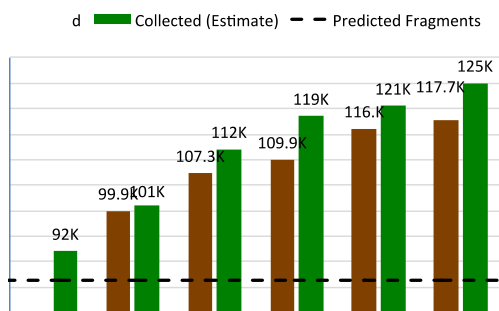

Fig. 19 Panel summary for FY2016

Fig. 20 Fragment summary for FY2016

Table 15 shows the average times for completing foam panels in the preparation, X-ray imaging, and extraction of debris fragments with at least one

---

* A total of 564 panels were installed in the test chamber. Because a number of panels were completely fragmented, the total number for processing is unclear until all are processed.

dimension as small as 2 mm. Some of the low-density panels have had close to 1,800 embedded debris fragments while some high-density panels have had zero embedded fragments.

Table 15 Breakdown of average times

	# of Panels	Average time (hr)
Panel preparation	369	3.0
X-ray imaging	312	0.5
Extraction	62	
Low density	12	15.2
Medium density	43	11.6
High density	7	9.4

As the DebriSat team continues the post-hypervelocity impact test activities in order to characterize massive amounts of fragments, the main challenge is the handling and working with the very small fragments. Fragments in the 2 mm range are very difficult to work with, thus, the technicians have been extremely careful and attentive during these efforts. To minimize handling of these fragments, automated measurement systems have been developed and implemented. Additionally, any human errors during measurements and data-entry are eliminated by utilizing the automated systems. Many of these tasks and activities are non-trivial, therefore, the procedures for each activity have been rigorously developed, implemented, and tested. Various parallel processing efforts have been implemented (e.g., multiple ergonomic extraction stations) for each activity and the DebriSat team is exploring alternative methods to expedite the characterization efforts while striving to maintain the highest integrity and value of the results. The team does not wish to produce unreliable results by unnecessarily expediting the processes. Thoughtful development and implementation are explored to further the current characterization process.

The first subset of fragments that have completed 2D imaging will be sent to NASA\JSC for further analyses. A subset of fragments will be analyzed in optical and radar facilities to further refine derived sizes from optical and radar cross sections, respectively. The data will ultimately be used to update existing break-up models used by NASA and DoD.

VI. REFERENCES
1. Rivero, M., Edhlund, I., Fitz-Coy, N., Liou, J.-C., Sorge, M., Huynh, T., Opiela, J., Cowardin, H., and

Krisko, P., "Hypervelocity Impact Testing of DebriSat to Improve Satellite Breakup Modeling," Proceedings of the 65th International Astronautical Congress, IAC-14-A6.2.10x25834, Toronto, Canada, September 2014.

2. Werremeyer, M., Clark, S., Fitz-Coy, N., Liou, J.-C., Sorge, M., Voelker, M., and Huynh, T., "Design and Fabrication of DebriSat - A Representative LEO Satellite for Improvements to Standard Satellite Breakup Models," Proceedings of the 63rd International Astronautical Congress, IAC-12,A6,3,7x16098, Naples, Italy, October 2012.

3. Rivero, M., Kleespies, J., Patankar, K., Fitz-Coy, N., Liou, J.-C., Sorge, M., Huynh, T., Opiela, J., Cowardin, H., and Krisko, P., "Characterization of Debris from the DebriSat Hypervelocity Test," Proceedings of the 66th International Astronautical Congress, IAC-15-A6.2.9x30343, Jerusalem, Israel, October 2015.

4. Kleespies, J., and Fitz-Coy, N., "Big Impacts and Big Data: Addressing the Challenges of Managing DebriSat's Characterization Data," Proceedings of the 2016 IEEE Aerospace Conference, Big Sky, MT, USA, March 5-12, 2016.

5. McKnight, D. S., Johnson, N. L., Fudge, M. L., and Maclay, T.D., "Satellite Orbital Debris Characterization Impact Test (SOCIT) Seris Data Collection Report," Kaman Sciences Corporation Report NAS9-19215, Alexandria, VA, 1995.

6. Moraguez, M., Patankar, K., Fitz-Coy, N., Liou, J.-C., Sorge, M., and Huyhn, T., "An Imaging System for Automated Characteristic Length Measurement of DebriSat Fragments," Proceedings of the 66th International Astronautical Congress, IAC-15-A6.1.30288, Jerusalem, Israel, October 12-15, 2015.

7. Moraguez, M., Patankar, K., Fitz-Coy, N., Liou, J.-C., and Cowardin, H, "An Imaging System for Satellite Hypervelocity Impact Deibris Characterization," Proceedings of The 2015 Advanced Maui Optical and Space Surveillance Technologies Conference, Maui, HI, USA, September 15-18, 2015.

8. Kutulakos, K. N. and Seitz, S. M., "A Theory of Shape by Space Carving," International Journal of Computer Vision 38(3), pp. 199-218, 2000.

9. Hanada, T., Liou, J.-C., Krisko, P., and Nakajima, T., "For Better Calculation of the Average Cross-Sectional Area of Breakup Fragments," Transactions of the Japan Society for Aeronautical and Space Sciences, Space Technology Japan, 2008-r-2-34, 2008.

10. "Measurement System Analysis – MSA Reference Manual," 4th Edition, Automotive Industry Action Group, 2010.

11. Duncan, A. J., "Values of d2 and d2," Quality Control and Industrial Statistics, 5th Edition, Appendix D3, January 1986.

12. Burdick, R. K., Borror, C. M., and Montogomery, D.C., "Design and Analysis of Gauge R&R Studies: Making Decisions with Confidence Intervals in Random and Mixed ANOVA Models," Society of Industrial and Applied Math, ISBN: 9780898715880, 2005.

13. "Repeatability and Reproducibility – Components of Variance, Percent of Tolerance, and Total Variation," StatSoft Inc. Website, 2015, [last visited: July 24, 2016].

14. "Gauge R&R study checks the suitability of your measurement system," Adaptive Business Management Systems Ltd. Website, [last visited: July 24, 2016].

15. "Average and Range Method," SAS/QC(R) 9.2 User's Guide Second Edition, SAS Institute Inc. Website, 2016, [last visited: July 24, 2016].

16. "Repeatability and Reproducibility," Engineered Software, Inc., 1999.